AIAA JOURNAL
Vol. 31, No. 5, May 1993

Numerical Study of Ignition Within Hydrogen-Air Supersonic Boundary Layers

Luís Fernando Figueira da Silva,* Bruno Deshaies,† and Michel Champion†
URA 193 au CNRS—ENSMA, 86034, Poitiers, France

Development of scramjet engines requires a better knowledge of the coupling between supersonic flow and combustion chemical kinetics. In this paper we consider a stationary uniform, laminar supersonic flow of a hydrogen-air mixture on a flat plate. Conditions of the flow at the outer edge of the boundary layer are chosen such that the chemical time is "infinitely" large when compared to the transit time over the computational domain. Ignition is triggered inside the boundary layer by viscous dissipation effects and/or wall temperature. This problem is solved numerically by a finite difference technique coupled with a chemical kinetics special solver and using classical boundary-layer assumptions, with two different types of boundary conditions: 1) adiabatic wall, and 2) constant temperature wall. Ignition of the reactive mixture within the boundary layer is observed as soon as either the freestream Mach number or the wall temperature are large enough. The combustion zone can be described as made up of three different regions, each of which depending on a particular coupling between chemical kinetics and fluid dynamics. The structure of this combustion zone is calculated for various freestream Mach numbers, different chemical kinetic mechanisms, reactive mixture equivalence ratios, and freestream and wall temperatures.

I. Introduction

CURRENT interest in the development of scramjet engines and ram accelerators has led to a renewal in the study of supersonic combustion phenomena. On a physical point of view, ignition and control of combustion within a supersonic flow give rise to a number of problems related to the coupling between a strongly exothermic chemistry and compressible, high-temperature, fluid dynamics.

The goal of the present numerical study is to investigate some aspects of the coupling between combustion chemical kinetics and viscous dissipation in strong shear regions of a supersonic combustor by considering a premixed hydrogen-air flow over an infinitely thin flat plate at zero angle of attack. The choice of hydrogen is justified because 1) it is the most likely fuel to be used in practical situations, and 2) from a theoretical point of view, it has a relatively well-known chemical scheme when compared to hydrocarbon fuels. The flow outside of the boundary layer is assumed to be uniform, supersonic, and with a static temperature low enough to be considered as chemically frozen. In this particular configuration we calculate the conditions under which ignition of the reactive mixture can be triggered within the laminar boundary layer by viscous dissipation and/or wall temperature effects. More precisely, and as a special feature of supersonic flows, ignition of the reactive mixture is shown to be the result of viscous dissipation only, in the case of an adiabatic wall but also under circumstances where both temperatures of the outer flow and the plate remain too small to trigger ignition. This is not the case in subsonic boundary layers, where the only way to ignite the mixture is to heat the plate.[1] The influence of dissipation effects was noted by Jackson and Hussaini,[2] relative to combustion development in a mixing layer. In the cases they investigated the shear seems to remain too small to induce ignition by itself, but led to a decrease on the ignition distance. It is clearly expected that these mechanisms are still relevant in the case of a turbulent flow even if turbulence should lead to quantitative changes in the results.

A finite difference technique, coupled to a complex chemical kinetics solver, is used along with the classical boundary-layer assumptions. Three different kinetic models are used and the conditions required for ignition of the reactive mixture are investigated as functions of the freestream Mach number, external flow temperature, wall temperature, and the equivalence ratio of the unburned mixture.

II. Mathematical Formulation

In the multicomponent flow that we consider, we neglect Dufour, Sorêt, and barodiffusion effects, bulk viscosity, and radiative heat transfer. Species diffusion is governed by Fick law. Classical boundary-layer approximations are used in the case of a multicomponent reactive flow. The condition to apply such approximations is that along the streamwise direction molecular transports remain much smaller than the convective transports. This implies that the characteristic length scale of the chemical process remains much larger than the typical length scale of the transverse gradients (the thickness of the boundary layer). This condition is always satisfied in a supersonic airstream—as shown in all of the figures represented in the present work—since for such a high-speed flow the chemical length scale becomes equal or smaller than the boundary-layer thickness only when the chemical time is equal or smaller than the molecular collision time. Under such assumptions the conservation equations for total mass, momentum, energy, and species read as[3]

$$\frac{\partial \rho u}{\partial x}+\frac{\partial \rho v}{\partial y}=0 \tag{1}$$

$$\rho u\frac{\partial u}{\partial x}+\rho v\frac{\partial u}{\partial y}=-\frac{\partial p}{\partial x}+\frac{\partial}{\partial y}\left(\mu\frac{\partial u}{\partial y}\right) \tag{2}$$

$$\frac{\partial p}{\partial y}=0 \tag{3}$$

Received Oct. 23, 1991; presented as Paper 92-0338 at the AIAA 30th Aerospace Sciences Meeting, Reno, NV, Jan. 6-9, 1992; revision received Sept. 18, 1992; accepted for publication Sept. 21, 1992.

*Graduate Student, Laboratoire d'Energétique et de Détonique, rue Guillaume VIII. Associate Member AIAA.

†Directeur de Recherches, Laboratoire d'Energétique et de Détonique, rue Guillaume VIII. Member AIAA.

$$\rho u c_p \frac{\partial T}{\partial x} + \rho v c_p \frac{\partial T}{\partial y} = u \frac{\partial p}{\partial x} + \frac{\partial}{\partial y}\left(\lambda \frac{\partial T}{\partial y}\right) - \sum_{\alpha=1}^{k} \rho Y_\alpha V_\alpha c_{p_\alpha} \frac{\partial T}{\partial y} + \mu\left(\frac{\partial u}{\partial y}\right)^2 - \sum_{\alpha=1}^{k} h_\alpha \omega_\alpha \quad (4)$$

$$\rho u \frac{\partial Y_\alpha}{\partial x} + \rho v \frac{\partial Y_\alpha}{\partial y} = -\frac{\partial}{\partial y}(\rho Y_\alpha V_\alpha) + \omega_\alpha \qquad \alpha = 1, \ldots, k \quad (5)$$

$$p = \rho R T \sum_{\alpha=1}^{k} \frac{Y_\alpha}{M_\alpha} \quad (6)$$

In these equations, x and y are the streamwise and transversal coordinates, u and v are the velocity vector components in these directions, T is the temperature, ρ is the mixture density, and p is the pressure.

For each of the k species, Y_α is the mass fraction, M_α the molecular weight, c_{p_α} the specific heat at constant pressure per unit of mass, and ω_α the production rate. The species specific enthalpy h_α is given by $h_\alpha = h_\alpha^0 + \int_{T_0}^{T} c_{p_\alpha}\, dT$. The production rates are given by Arrhenius laws whose description and calculation procedure are those of Kee et al.[4] V_α is the diffusion velocity and D_α is the diffusion coefficient, related by $\rho Y_\alpha V_\alpha = -\rho D_\alpha \partial Y_\alpha / \partial y$. The mixture molecular viscosity, thermal conductivity, and specific heat at constant pressure per unit of mass are μ, λ, and c_p, respectively, and R is the universal gas constant. These transport coefficients and thermodynamic properties are calculated as functions of local values for temperature, pressure, and composition through the computer package provided by Kee et al.[4,5]

Boundary conditions at $x = x_0$ are the Blasius compressible nonreacting self-similar boundary-layer values[6] for u, T, and ρ. The values of Y_α are those corresponding to the mixture composition in the outer flow for a given equivalence ratio. The boundary conditions at infinity for the cross-stream coordinate y are those corresponding to undisturbed freestream conditions (fixed u_∞, T_∞, p_∞, and $Y_{\alpha\infty}$). Concerning the wall condition at $y = 0$, two kinds of boundary conditions are considered: an adiabatic wall and a constant temperature wall. It must be noticed that catalytic effects at the wall are not considered. The subscripts ∞ and u correspond to freestream and wall conditions, respectively.

Equations (1-6) are modified using the von Mises[6] coordinate transformation; i.e., $(x, y) \rightarrow (x^*, \psi)$, with $\rho u = \partial\psi/\partial y$, $\rho v = -\partial\psi/\partial x$, leading to a more convenient set of parabolic partial differential equations.

Since only the case of an infinitely thin flat plate with zero angle of attack is considered, the streamwise pressure gradient is fixed by the flow conditions at the outer edge of the boundary layer. This allows the use of a marching numerical procedure in the streamwise direction. Only the case of constant pressure flow is considered in this paper.

III. Numerical Procedure

The transformed equations are discretized using first-order implicit finite differences for the marching direction and second-order implicit finite differences for the ψ coordinate. This results in a system of nonlinear equations that we solve by using a modified damped Newton method. The code that we use is a modified version of the one provided by Kee et al.,[7] and originally tailored for the solution of planar stationary flames. Further details about the method can be found in Deuflhard[8] and Curtis et al.[9]

A mesh rezoning method is used in the ψ coordinate. The mesh is locally halfed periodically, when the gradient and the curvature of the solution overcome certain thresholds. The mesh rezoning code is the one used by Kee et al.[7] The mesh spacing in the x direction is fixed, and care must be taken that it does capture the small chemical lengths provoking the stiffness of the problem.

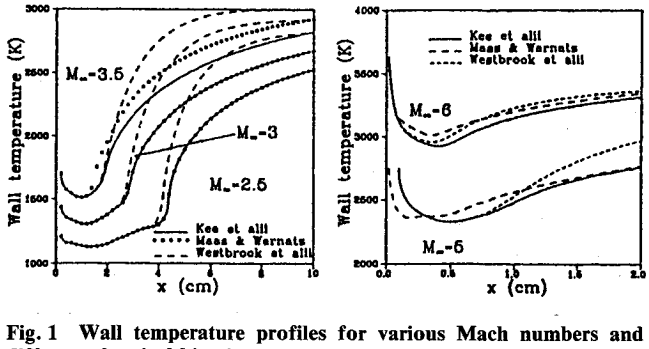

Fig. 1 Wall temperature profiles for various Mach numbers and different chemical kinetics.

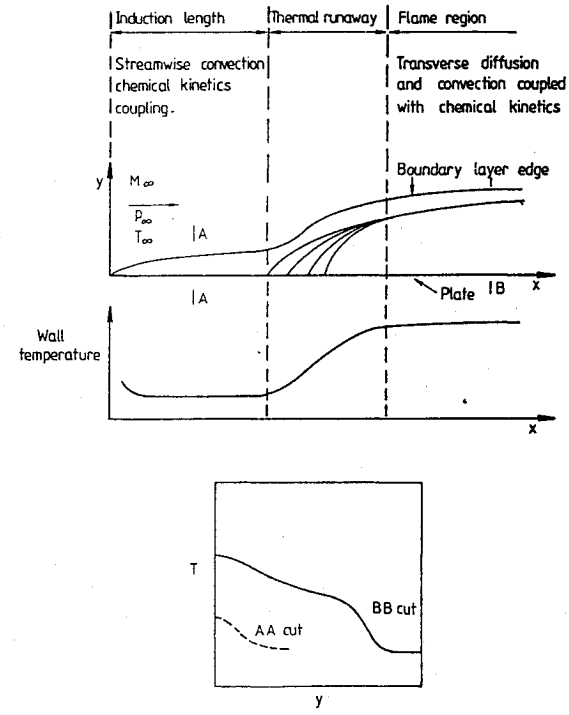

Fig. 2 Schematic representation of the boundary layer.

IV. Results and Discussion

In a previous work[10] a validation of the computer code was performed, comparing the results for nonreactive boundary layers with excellent agreement.

Ignition and Spread of Combustion in a Supersonic Boundary Layer

As the supersonic premixed gases reach the flat plate, they heat up in the boundary layer. This heating is due to viscous dissipation, and so increases with the freestream Mach number. The mixture starts reacting, leading eventually to a thermal runaway characterized by a large temperature increase. The distance for such a thermal runaway to occur is the induction length. This behavior is illustrated by Fig. 1 showing the change of wall temperature with the streamwise distance, in the case of an adiabatic plate. It must be noticed that the steep temperature decrease at the very beginning of the plate is due to adjustments of the physical coefficients in the equations, the most important being that of the specific heat.

The structure of the boundary layer, illustrated in Fig. 2, can be described as made of three regions:

1) An induction zone controlled by initiation and chain-branching reactions, where the temperature is mainly controlled by viscous dissipation, the influence of the chemical kinetics remaining weak. In this zone, convection balances chemical production with a transverse smoothing effect due to molecular transports.

2) A thermal runaway zone, where the chain-branching and propagation reactions with large activation energies eventually

lead to an important heat release associated with recombination reactions. This heat release is responsible for the thickening of the boundary layer.

3) A zone where a strongly oblique flame is positioned. This flame is controlled by a balance between transverse molecular transports, convection, and chemistry.

Since here we treat only the case of an unconfined flow, the boundary layer is free to thicken after the beginning of the heat release. This is illustrated in Fig. 2. The thickening becomes less important with increasing Mach numbers, as the system tends globally to endothermicity (species dissociate, but do not recombine, due to the high initial temperatures).

In the confined case (not studied here, but object of future work), the streamwise gradients induced by the thermal runaway can produce an oblique shock wave that could lead to a thermal runaway of the whole flow.

Table 1 Reaction mechanism according to Kee et al.[7] [$k_f = AT^\beta \exp(-E/RT)$]

Reaction	A, cm · mole · s	β	E, cal/mole
$H + O_2 \rightleftharpoons OH + O$	5.13E16	−0.816	16,507
$O + H_2 \rightleftharpoons OH + H$	1.80E10	1.00	8,826
$OH + H_2 \rightleftharpoons H_2O + H$	1.17E09	1.30	3,626
$OH + OH \rightleftharpoons O + H_2O$	6.00E08	1.30	0
$H_2 + M \rightleftharpoons H + H + M^a$	2.23E12	0.50	92,600
$H + OH + M \rightleftharpoons H_2O + M^b$	7.50E23	−2.60	0
$O_2 + M \rightleftharpoons O + O + M$	1.85E11	0.50	95,560
$H + O_2 + M \rightleftharpoons HO_2 + M^c$	2.10E18	−1.00	0
$H + HO_2 \rightleftharpoons OH + OH$	2.50E14	0.00	1,900
$H + HO_2 \rightleftharpoons H_2 + O_2$	2.50E13	0.00	700
$H_2 + O_2 \rightleftharpoons OH + OH$	1.70E13	0.00	47,780
$O + HO_2 \rightleftharpoons O_2 + OH$	4.80E13	0.00	1,000
$OH + HO_2 \rightleftharpoons H_2O + O_2$	5.00E13	0.00	1,000
$HO_2 + HO_2 \rightleftharpoons H_2O_2 + O_2$	2.00E12	0.00	0
$H_2O_2 + M \rightleftharpoons OH + OH + M$	1.30E17	0.00	45,500
$H_2O_2 + H \rightleftharpoons HO_2 + H_2$	1.60E12	0.00	3,800
$H + O_2 + O_2 \rightleftharpoons HO_2 + O_2$	6.70E19	−1.42	0
$H + O_2 + N_2 \rightleftharpoons HO_2 + N_2$	6.70E19	−1.42	0
$H_2O_2 + OH \rightleftharpoons H_2O + HO_2$	1.00E13	0.00	1,800

Third-body efficiencies: $f_{N_2} = f_{O_2} = 0$. [a] $-f_{H_2O} = 6$, $f_H = 2$, $f_{H_2} = 3$. [b] $f_{H_2O} = 20$, [c] $-f_{H_2O} = 21$, $f_{H_2} = 3.3$.

Table 2 Reaction mechanism according to Maas and Warnatz[11] [$k_f = AT^\beta \exp(-E/RT)$]

Reaction	A, cm · mole · s	β	E, cal/mole
$O_2 + H \rightleftharpoons OH + O$	2.20E14	0.00	16,818
$H_2 + O \rightleftharpoons OH + H$	5.06E04	2.67	6,292
$H_2 + OH \rightleftharpoons H_2O + H$	1.00E08	1.60	3,301
$OH + OH \rightleftharpoons H_2O + O$	1.50E09	1.14	96
$H + H + M \rightleftharpoons H_2 + M$	1.80E18	−1.00	0
$H + OH + M \rightleftharpoons H_2O + M$	2.20E22	−2.00	0
$O + O + M \rightleftharpoons O_2 + M$	2.90E17	−1.00	0
$H + O_2 + M \rightleftharpoons HO_2 + M$	2.30E18	−0.80	0
$HO_2 + H \rightleftharpoons OH + OH$	1.50E14	0.00	1,005
$HO_2 + H \rightleftharpoons H_2 + O_2$	2.50E13	0.00	694
$HO_2 + H \rightleftharpoons H_2O + O$	3.00E13	0.00	1,722
$HO_2 + O \rightleftharpoons OH + O_2$	1.80E13	0.00	−407
$HO_2 + OH \rightleftharpoons H_2O + O_2$	6.00E13	0.00	0
$HO_2 + HO_2 \rightleftharpoons H_2O_2 + O_2$	2.50E11	0.00	−1,244
$OH + OH + M \rightleftharpoons H_2O_2 + M$	3.25E22	−2.00	0
$H_2O_2 + H \rightleftharpoons H_2 + HO_2$	1.70E12	0.00	3,756
$H_2O_2 + H \rightleftharpoons H_2O + OH$	1.00E13	0.00	3,589
$H_2O_2 + O \rightleftharpoons OH + HO_2$	2.80E13	0.00	6,412
$H_2O_2 + OH \rightleftharpoons H_2O + HO_2$	5.40E12	0.00	1,005

Third-body efficiencies: $f_{H_2} = 1.0$, $f_{O_2} = 3.5$, $f_{H_2O} = 6.5$, $f_{N_2} = 0.50$.

Table 3 Reaction mechanism according to Westbrook and Dryer[12] [$k_f = AT^\beta \exp(-E/RT)$]

Reaction	A, cm · mole · s	β	E, cal/mole
$H + O_2 \rightleftharpoons O + OH$	5.13E16	−0.816	16,510
$O + H_2 \rightleftharpoons H + OH$	1.81E10	1.00	8,900
$H_2 + OH \rightleftharpoons H_2O + H$	2.20E13	0.00	5,150
$O + H_2O \rightleftharpoons OH + OH$	6.76E13	0.00	18,360
$H + H + M \rightleftharpoons H_2 + M$	3.02E15	0.00	0
$H + OH + M \rightleftharpoons H_2O + M$	1.41E23	−2.00	0
$O + O + M \rightleftharpoons O_2 + M$	1.91E11	0.00	−1,790
$H + O_2 + M \rightleftharpoons HO_2 + M$	1.51E15	0.00	−1,000
$H + HO_2 \rightleftharpoons OH + OH$	2.51E14	0.00	1,900
$H + HO_2 \rightleftharpoons H_2 + O_2$	2.51E13	0.00	700
$H + HO_2 \rightleftharpoons H_2O + O$	5.01E13	0.00	1,000
$HO_2 + O \rightleftharpoons O_2 + OH$	5.01E13	0.00	1,000
$HO_2 + OH \rightleftharpoons H_2O + O_2$	5.01E13	0.00	1,000
$HO_2 + HO_2 \rightleftharpoons H_2O_2 + O_2$	1.00E13	0.00	1,000
$H_2O_2 + M \rightleftharpoons OH + OH + M$	1.20E17	0.00	45,500
$H_2O_2 + H \rightleftharpoons HO_2 + H_2$	1.70E12	0.00	3,750
$H_2O_2 + H \rightleftharpoons H_2O + OH$	3.16E14	0.00	8,940
$O + H + M \rightleftharpoons OH + M$	1.00E16	0.00	0
$H_2O_2 + OH \rightleftharpoons H_2O + HO_2$	1.00E13	0.00	1,800
$O + OH + M \rightleftharpoons HO_2 + M$	1.00E17	0.00	0
$H_2 + O_2 \rightleftharpoons OH + OH$	2.51E12	0.00	38,950

Influence of the Chemical Kinetics Scheme

To test the influence of the kinetic scheme on the flow structure, we select three mechanisms which are considered to be representative of the H_2-air combustion and listed in Tables 1-3. In these chemical schemes N_2 is treated as an inert. As evidenced below, the combustion process will be modified significantly by N_2 dissociation only for combustion temperatures higher than 3000 K. Each of the chemical schemes we use involves nine species—H_2, O_2, H_2O, OH, H, O, HO_2, H_2O_2, and N_2. The forward reaction rates are given by k_f, and the corresponding reaction rates ω_α are calculated according to Ref. 4.

The tests are performed with $T_\infty = 700$ K, $p_\infty = 0.1$ MPa, a unity equivalency ratio ϕ, and for Mach number ranging from 2 to 6. Calculations are performed up to a value of the streamwise coordinate $x = 10$ cm.

In Fig. 1 we can observe that, during the induction period, the three kinetic schemes yield the same streamwise temperature profiles for low Mach numbers. For higher freestream Mach numbers, it is observed that the Maas and Warnatz[11] chemical scheme yields a shorter induction length than the two others. Notice that for these high Mach numbers the induction region becomes more difficult to characterize since, due to high dissociation of the products, the thermal runaway and the heat released by the chemical process are of small amplitude. More precisions concerning these high Mach number cases will be given in the next section. The induction length, taken as the distance at which H_2O mass fraction is 50% of its maximum value, is given as a function of the freestream Mach number in Fig. 3. This figure confirms the points just discussed. Typical mass fraction profiles are given in Fig. 4. They clearly indicate that at the beginning of the induction zone HO_2 mass fraction is of the same order of magnitude as O, H, and OH.

A simple sensitivity analysis indicates that the decrease of the induction length observed with the Maas and Warnatz[11] kinetics is principally due to the difference in kinetics constants characterizing reaction $H + O_2 \rightleftharpoons OH + O$. This is illustrated by Fig. 5 where the wall temperature evolution at Mach 3.5 is shown; calculations are made with the original schemes and by changing, in the Maas and Warnatz[11] scheme, the constants of the just-cited reaction by its values on the Kee et al.[7] scheme. Concerning the thermal runaway region, it is

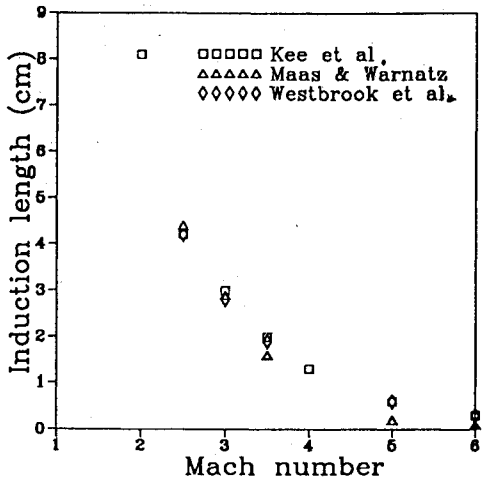

Fig. 3 Induction length as a function of the Mach number for different chemical kinetics.

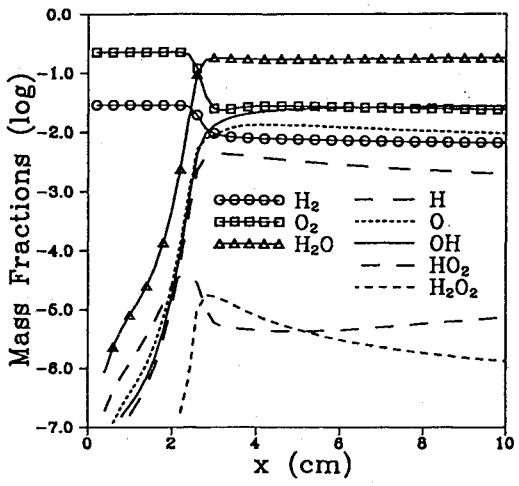

Fig. 4 Mass fractions profiles at the wall (Mach 3).

observed (Fig. 1) that the Westbrook and Dryer[12] kinetics scheme leads to a faster temperature rise. In Fig. 5 we also show the wall temperature evolution at Mach 3.5, with the original schemes of Kee et al.[7] and Westbrook and Dryer[12] and with the constants of the reaction $H + OH + M \rightleftharpoons H_2O + M$ substituted in the latter scheme by its values in the former. It is clear that this difference is partly due to this recombination reaction. A much more detailed sensitivity analysis, which is out of the scope of this paper, would be needed to provide a full comprehensive explanation of these differences.

Influence of the Freestream Mach Number on the Structure of the Boundary Layer

In Fig. 6, the wall temperature is plotted at $x = 10$ cm and therefore in the flame zone. In the same figure, the temperature of the wall in the absence of any chemical process is also plotted. For a Mach number $M_\infty = 6$, it can be observed that the maximum flow temperature is lower in the case with combustion than in the one without combustion, which means that, due to dissociation effects, the whole combustion behaves as an endothermic process for large values of the freestream Mach number. Figure 6 also shows the calculations performed for air only, with and without dissociation at $x = 10$ cm. One can see that a significant nitrogen dissociation is obtained only for temperature larger than 3000 K. This result justifies the choice of treating N_2 as an inert, in the whole combustion process, within the range of combustion temperatures considered in the present work. A study of pollutant formation, where NO_x radicals are important, certainly

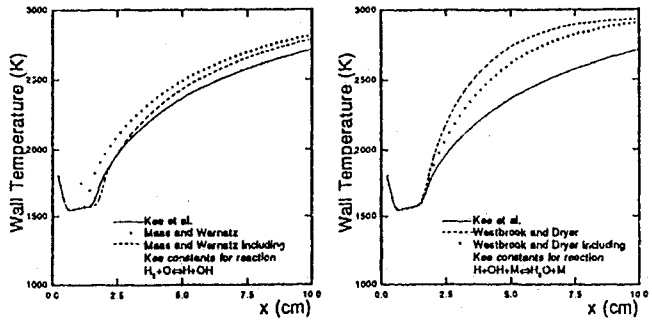

Fig. 5 Wall temperature profiles for Mach number 3.5 (Kee et al.[7] vs Maas and Warnatz,[11] Westbrook and Dryer kinetics[12]).

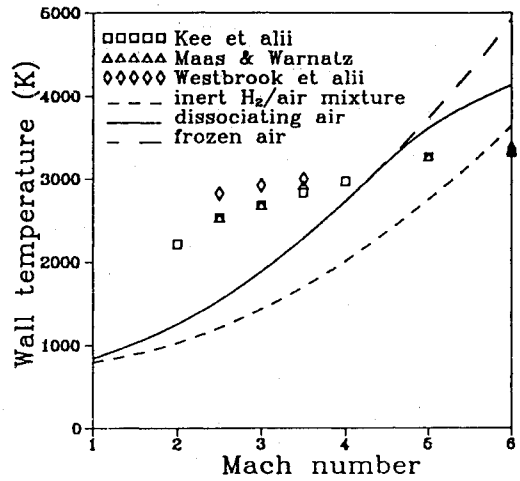

Fig. 6 Wall temperature at $x = 10$ cm as a function of the Mach number for the different chemical kinetics.

requires a more careful study involving N_2 chemistry. The chemical kinetics scheme used for air is the one used by Mitchell and Kee,[13] shown in Table 4.

The influence of the freestream Mach number can be further illustrated by Fig. 7, where transversal temperature profiles are plotted adimensionalized by T_∞ as functions of the boundary-layer coordinate η ($\eta = y\sqrt{U_\infty \rho_\infty / \mu_\infty x}$) at $x = 2$ and 10 cm, for Mach numbers from 2 to 6. As shown in Fig. 7 for $x = 10$ cm, the flame is positioned at the edge of the boundary layer, and there is an additional increase of heat release due to friction which leads to a temperature above the adiabatic flame temperature (here 2580 K) near the wall.

Influence of Equivalence Ratio and Temperature of the Outer Flow

We performed a limited investigation of the influence of the mixture equivalence ratio and the outer flow temperature on ignition. In addition to the stoichiometric case, two equivalence ratios, 0.5 and 2.0, were chosen as representative of a lean and a rich combustible mixture, respectively. Two freestream static temperatures, 400 and 700 K, were used as boundary conditions. As the ignition mechanism is not qualitatively modified by the choice among the three chemical schemes tested, from here on we retain the one provided by Kee et al.[7] only. Static pressure remains fixed to 0.1 MPa.

In Fig. 8, wall temperatures are given as functions of the streamwise coordinate x for different values of the equivalence ratio and freestream Mach number. Figure 9 shows the influence of the freestream temperature on the wall temperature profile. As expected, these results show that the lower the temperature of the outer flow, the longer the induction length. Not so trivial is the influence of the equivalence ratio on the induction length: the lean mixture is found to have the shorter induction length, although it is less energetic than both the

Table 4 Air reaction mechanism according to Mitchell and Kee[13] [$k_f = AT^{\beta} \exp(-E/RT)$]

Reaction	A, cm · mole · s	β	E, cal/mole
$N_2 + O_2 \rightleftharpoons NO + NO$	9.10E24	−2.5	128,500
$N_2 + O \rightleftharpoons NO + N$	7.00E13	0.0	75,000
$O_2 + N \rightleftharpoons NO + O$	1.34E10	1.0	7,080
$O_2 + M \rightleftharpoons O + O + M^a$	3.62E18	−1.0	118,000
$N_2 + M \rightleftharpoons N + N + M^b$	1.92E17	−0.5	224,900
$N_2 + N \rightleftharpoons N + N + N$	4.10E22	−1.5	224,900
$NO + M \rightleftharpoons N + O + M^c$	4.00E20	−1.5	150,000

Third-body efficiencies: $^a f_{N_2} = 2$, $f_{O_2} = 9$, $f_O = 25$. $^b f_{N_2} = 2.5$, $f_N = 0$. $^c f_{NO} = 20$, $f_O = 20$, $f_N = 20$.

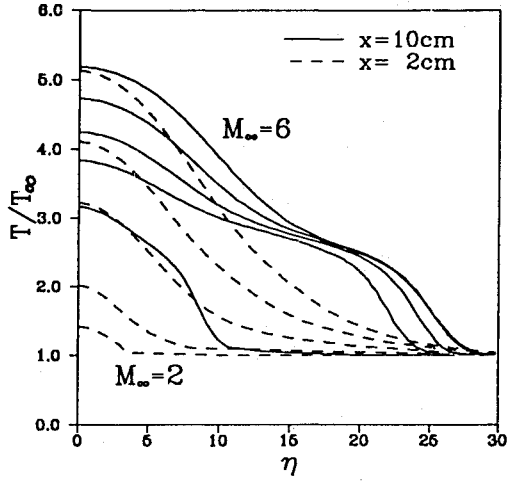

Fig. 7 Transversal temperature profiles for Mach numbers 2 to 6.

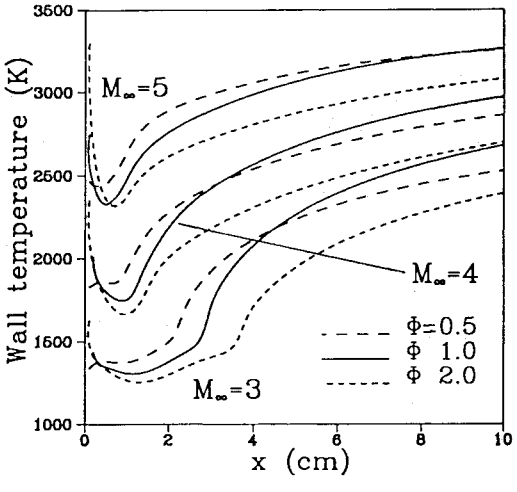

Fig. 8 Wall temperature profiles for various Mach numbers and different equivalence ratios.

stoichiometric and the rich mixtures used in our test. This result can be explained by noticing that the specific heat of the mixture increases with the equivalence ratio. As a consequence, the heating which occurs at the beginning of the boundary layer is more intense in the case of lean mixtures, thus decreasing the induction length.

Case of a Constant Temperature Wall

We consider now the case where the temperature of the flat plate is constant. Two different cases are studied where wall temperature is fixed: 1) to the value of the freestream static temperature (700 K), and 2) the adiabatic wall temperature T_{ad} obtained in the absence of any chemical process. The transversal profiles of temperature are shown in Fig. 10 at two streamwise positions, $x = 2$ and 10 cm.

For case 1 shown in Fig. 10, ignition is only obtained within the range of abscissa $0 < x < 10$ cm when the freestream Mach number reaches relatively high values, i.e., 5.5 and 6. In this case, the wall serves as a heat sink, preventing combustion from developing at the wall. In such a configuration, of great interest in practical applications, ignition occurs in the central part of the boundary layer. One important parameter for actual combustors is the intensity of the heat transfer to the

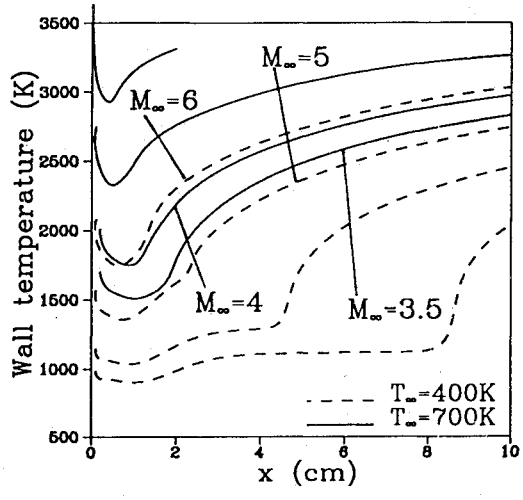

Fig. 9 Wall temperature profiles for various Mach numbers and different freestream temperatures.

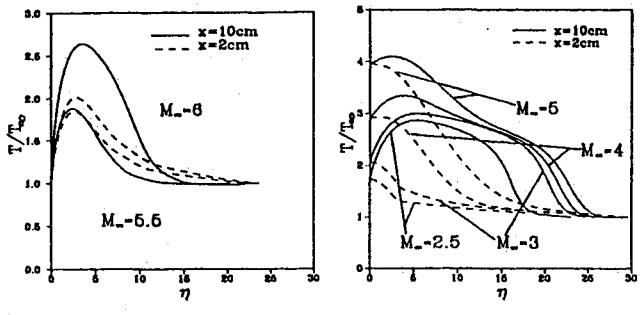

Fig. 10 Transversal temperature profiles for various Mach numbers at two streamwise positions: a) $T_w = T_\infty$; and b) $T_w = T_{ad}$.

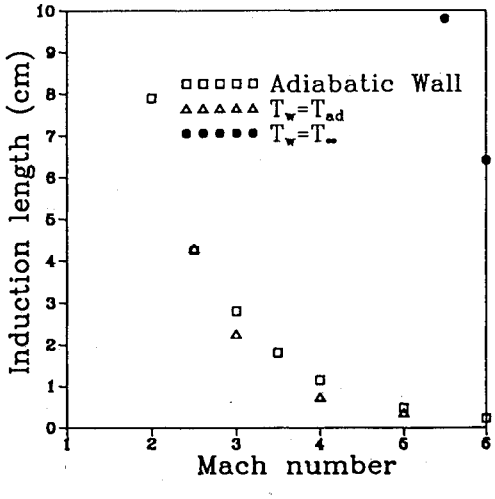

Fig. 11 Induction length for various wall conditions.

wall. The magnitude of this heat transfer is given by the slopes of the curves at $\eta = 0$. A thorough investigation is now being performed.

For case 2 shown in Fig. 10, ignition is obtained for all Mach numbers studied but two. We see that the slope of the curves and therefore the heat transfer $[q_w = -\lambda(\partial T/\partial y)_0]$ at $x = 10$ cm decreases as the Mach number increases. In Fig. 11, induction lengths are plotted as functions of the freestream Mach number for the adiabatic wall and for cases 1 and 2. The induction lengths for case 1 are much larger, as expected, whereas those for case 2 are slightly shorter than those of the adiabatic wall. This latter result can be explained in view of Fig. 1: as the wall temperature is fixed, the induction period is characterized by the heat transfer from the wall to the fluid, this being responsible for a faster thermal runaway.

Parametric Study of the Ignition within a Boundary Layer

In view of the results described in the preceding sections, a parametric study was performed to determine the occurrence of ignition within the boundary layer developing over a 10-cm-long flat plate. For this purpose, ignition is considered to occur as soon as the H_2O mass fraction becomes greater than 2.5×10^{-2}. Such a value is observed to correspond to the beginning of the thermal runaway.

Following this criterion, Figs. 12 and 13 give mappings of ignition curves in the (M_∞, T_∞) plane for various values of equivalence ratio (Fig. 12) and wall temperature (Fig. 13). The trends observed in the preceding paragraphs concerning the effect of equivalence ratio and wall temperature are confirmed by these figures in plausible ranges of T_∞ and M_∞. It should be noticed that increasing the freestream Mach number at fixed chemical time leads to an increase of the induction length. On the other hand, increasing the freestream Mach number results in an increase of the viscous dissipation and therefore in a decrease of the chemical induction time. For all of the cases investigated, this configuration always leads to a decrease of the induction length, except for the one given in Fig. 13 corresponding to $T_w = 1100$ K. If for this case ignition always occurs for a value of T_∞ larger than about 450 K, for lower values of T_∞ there exists a range where, simultaneously, convection is too large and viscous dissipation is too small for ignition to be observed before the end of the plate.

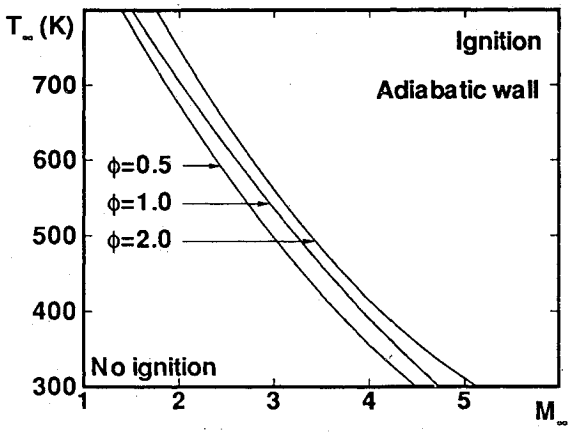

Fig. 12 Ignition curves in the (M_∞, T_∞) plane for different wall temperatures. Case of an adiabatic 10-cm flat plate.

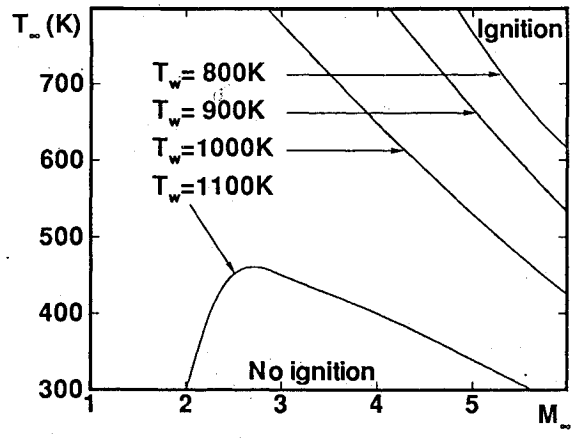

Fig. 13 Ignition curves in the (M_∞, T_∞) plane for different wall temperatures. Case of a stoichiometric H_2/air mixture flowing over a 10-cm flat plate.

V. Conclusions

We present a numerical study of the ignition and spread of combustion within a supersonic boundary layer, in cases where ignition is triggered by viscous dissipation and/or wall temperature effects. It is shown that ignition of a reactive mixture can be obtained as a result of viscous dissipation effects only, in a supersonic boundary-layer flow over an adiabatic wall, but also under circumstances where both the temperatures of the outer flow and the plate remain too small to induce ignition of the mixture.

In the case of $T_\infty = 700$ K, unitary equivalence ratio, and adiabatic wall, ignition is obtained as soon as the freestream Mach number is greater than 2. In the case of a constant temperature wall, it is shown that ignition can be avoided by setting up the wall temperature equal to the freestream temperature in the range of Mach numbers studied up to 5.5.

In the streamwise direction three important regions are found in the boundary layer. These three regions are as follows:

1) An induction region where the process is mainly controlled by streamwise convection and chemical kinetics in the presence of transverse molecular transports. These transverse transports effects being excepted, this problem is very similar to the Semenov explosion and leads to the existence of an induction length for the combustion process.

2) A thermal runaway region corresponding to a large chemical heat release.

3) A flame region which develops at the end of the thermal runaway region where a flame is stabilized at the outer edge of the boundary layer.

This splitting of the space is more evident for low Mach numbers, i.e., up to 4 when $T_\infty = 700$ K. It is clear that decreasing the freestream temperature will increase the freestream Mach number limit where this splitting remains evident. This disappearance of three distinguishable regions is due to an increase in dissociation effects on the burned gases for large combustion temperatures and large freestream Mach numbers. In the limit of large values of the freestream Mach number, the whole chemical process is found to become endothermic. In such cases, the wall temperature is smaller when "combustion" develops in the boundary layer than in the case of a chemically free flow.

For a given freestream Mach number, the induction length is found to be an increasing function of the equivalence ratio. The various chemical kinematics schemes used lead to the same qualitative results concerning the structure of the flow and the leading mechanism, but both the induction length and temperature rise in the thermal runaway region are found to be affected.

Results concerning the effects of freestream temperature T_∞, freestream Mach number M_∞, equivalence ratio of the mixture ϕ, and wall temperature T_w are summarized by mappings of ignition curves in the ranges $300 \leq T_\infty \leq 800$ K, $1 \leq M_\infty \leq 6$, $0.5 \leq \phi \leq 2.0$, and $800 \leq T_w \leq 1100$ K.

Acknowledgment

The authors wish to thank the Société Européene de Propulsion for its financial support.

References

[1]Treviño, C., and Méndez, F., "Asymptotic Analysis of the Ignition of Hydrogen by a Hot Plate in a Boundary-Layer Flow," *Combustion Science and Technology,* Vol. 78, Nos. 4–6, 1991, pp. 197–216.

[2]Jackson, T. L., and Hussaini, M. Y., "An Asymptotic Analysis of Supersonic Reacting Mixing Layers," *Combustion Science and Technology,* Vol. 57, Nos. 4–6, 1988, pp. 129–140.

[3]Williams, F. A., *Combustion Theory,* 2nd ed., Benjamin/Cummings Publishing Co., Menlo Park, CA, 1985.

[4]Kee, R. J., Miller, J. A., and Jefferson, T. H., "CHEMKIN: A General-Purpose, Problem-Independent, Transportable, Fortran Chemical Kinetics Code Package," Sandia National Labs., SAND80-8003/UC-4, Albuquerque, NM, March 1980.

[5]Kee, R. J., Warnatz, J., and Miller, J. A., "A Fortran Computer Code Package for the Evaluation of Gas-Phase Viscosities, Conductivities, and Diffusion Coefficients," Sandia National Labs., SAND83-8209/UC-32, Albuquerque, NM, March 1983.

[6]Schlichting, H., *Boundary Layer Theory,* 7th ed., McGraw-Hill, New York, 1979.

[7]Kee, R. J., Grcar, J. F., Smooke, M. D., and Miller, J. A., "A Fortran Program for Modeling Steady Laminar One-Dimensional Premixed Flames," Sandia National Labs., SAND85-8240/UC-4, Albuquerque, NM, Dec. 1985.

[8]Deuflhard, P., "A Modified Newton Method for the Solution of Ill-Conditioned Systems of Nonlinear Equations with Application of Multiple Shooting," *Numerical Mathematics,* No. 22, 1974, pp. 289–315.

[9]Curtis, A. R., Powell, M. J., and Reid, J. K., "On the Estimation of Sparse Jacobian Matrices," *Journal of the Institute of Mathematics Applications,* No. 13, 1974, pp. 117–119.

[10]Figueira da Silva, L. F., Deshaies, B., and Champion, M., "Ignition and Spread of Combustion within a Supersonic Boundary Layer," *Combustion and Reaction Kinetics—22nd International Annual Conference of ICT,* Fraunhofer-Institut für Chemische Technologie, Karlsruhe, FRG, July 1991.

[11]Maas, U., and Warnatz, J., "Ignition Process in Hydrogen-Oxygen Mixtures," *Combustion and Flame,* Vol. 74, No. 1, 1988, pp. 53–69.

[12]Westbrook, C. K., and Dryer, F. L., "Chemical Kinetic Modeling of Hydrocarbon Combustion," *Progress in Energy and Combustion Science,* Vol. 10, No. 1, 1984, pp. 1–57.

[13]Mitchell, R. E., and Kee, R. J., "A General-Purpose Computer Code for Predicting Chemical Kinetic Behavior Behind Incident and Reflected Shocks," Sandia National Labs., SAND82-8205, Albuquerque, NM, March 1982.